ENGINEERING APPLICATIONS OF COMPUTATIONAL FLUID MECHANICS, 2017
VOL. 11, NO. 1, 30–41
http://dx.doi.org/10.1080/19942060.2016.1235515

Taylor & Francis
Taylor & Francis Group

Active flow control of the vortex rope and pressure pulsations in a swirl generator

Ardalan Javadi and Håkan Nilsson

Division of Fluid Dynamics, Department of Applied Mechanics, Chalmers University of Technology, Göteborg, Sweden

ABSTRACT

The vortex rope and pressure pulsations caused by a radial pressure gradient in the conical diffuser of a swirl generator is controlled using continuous slot jets with different momentum fluxes and angles injected from the runner crown. The swirl apparatus is designed to generate flows similar to those in the different operating conditions of a Francis turbine. The study is done with numerical modelling using the hybrid URANS-LES (Unsteady Reynolds-Averaged Navier–Stokes–Large Eddy Simulation) method with the rotor–stator interaction. The comprehensive studies of Javadi and Nilsson [Time-accurate numerical simulations of swirling flow with rotor–stator interaction. *Flow, Turbulence and Combustion*, Vol. 95, pp. 755–774], and Javadi, Bosioc, Nilsson, Muntean and Susan-Resiga [Experimental and numerical investigation of the precessing helical vortex in a conical diffuser, with rotor–stator interaction. *ASME Journal of Fluids Engineering*, doi:10.1115/1.4033416] are considered as the bench mark, and the capabilities of the technique is studied in the present work with the validated numerical results presented in those studies. The pressure pulsations caused by the pressure gradient generated by the swirl, present at off-design conditions, are cumbersome for hydropower structures. The investigation shows that the pressure pulsation, velocity fluctuations and the size of the vortex rope decrease when the jet is injected from the runner crown. The flow rate of the jet is less than 3% of the flow rate of the swirl generator. The momentum flux, angle of injection of the jet and the position of the slot are important factors for the effectiveness of the flow control technique.

ARTICLE HISTORY
Received 11 March 2016
Accepted 7 September 2016

KEYWORDS
Flow control; vortex rope; hybrid URANS-LES; rotor–stator interaction

1. Introduction

A main source of loss in Francis turbines is the on-axis stagnant region and the ensuing helical vortex rope in the draft tube. The flow in water turbines operating at the best efficiency point condition has a moderately low level of swirl forming a stable on-axis structure (Javadi, Bosioc, Nilsson, Muntean, & Susan-Resiga, 2016; Javadi & Nilsson, 2015a). The flow at conditions away from the best efficiency point often contains a high level of swirl which may cause a recirculation region. The recirculation region may break down the stable on-axis structure formed at the best efficiency point. This vortex breakdown initiates a so-called precessing helical vortex rope. Prevention of the vortex breakdown or mitigation of the pressure pulsations can significantly enhance the stability of the flow and decrease the level of unsteadiness in the draft tube. Nishi, Wang, Yoshida, Takahashi, and Tsukamoto (1996) used fins to mitigate the pulsation in the draft tube. They showed that using fins on the draft tube wall may increase the operating range of a Francis turbine. Kjeldsen, Olsen, Nielsen and Dahlhaug (2006) proposed a method to decrease the pressure pulsations in a Francis turbine draft tube by injecting high speed water jets from distributed positions from the draft tube walls. The jets were injected circumferentially and yawed downstream with respect to the machine axis. The volume flow rate of the water used is however very high in that method, which decreases the efficiency of the machine. Recently, the injection of a continuous jet from the runner crown centre was studied by Susan-Resiga, Muntean, Hasmatuchi, Anton, and Avellan (2010), Susan-Resiga, Vu, Muntean, Ciocan, and Nennemann (2006), and Tănasă, Bosioc, Muntean, and Susan-Resiga (2013). The method mitigates the pressure drop in the draft tube and removes the vortex rope by flushing it downstream with the jet. This leads to a remarkable reduction of the pulsations in the draft tube, but still at the cost of a high flow rate in the jet. Tănasă et al. (2013) used a flow-feedback method with the water taken from downstream in the draft tube to keep the nominal discharge constant. Rusak, Granata, and Wang (2015) studied a flow injection distributed

CONTACT Ardalan Javadi ardalan.javadi@chalmers.se

along a finite-length straight circular pipe wall to control the vortex breakdown process in incompressible axisymmetric swirling flows. They demonstrated that applying the proposed control method during flow evolution is successful in eliminating the breakdown states. All the research works mentioned above were performed experimentally, which is accurate but more expensive than numerical investigations of similar flow fields.

Large Eddy Simulation (LES) is very expensive for wall-bounded flows at practical Reynolds numbers. The hybrid URANS-LES (Unsteady Reynolds-Averaged Navier–Stokes–LES) approach is a mix of URANS and LES modes. This approach removes the requirements of fine resolutions in wall-parallel directions for a well-resolved LES. Javadi and Nilsson (2014a) studied the Scale-Adaptive Simulation (SAS) (Menter & Egorov, 2010) approach in highly swirling flows and reported that the approach predicts the massively separated swirling flows very well. Detached-Eddy Simulation (DES) (Spalart, Jou, Strelets, & Allmaras, 1997) is another promising hybrid URANS-LES strategy which is studied for application to swirling flows (Javadi & Nilsson, 2015a, 2015b; Javadi et al., 2016). The Delayed DES (DDES) methodology was proposed by Spalart et al. (2006) to identify the boundary layer thickness and to extend the URANS mode compared to that of the initially proposed DES methodology. DDES protects the boundary layer from the LES mode even if a coarse wall-parallel grid spacing would normally activate the DES limiter (Spalart, 2009). This method is appropriate for flows with large internal structures at practical Reynolds numbers. Javadi and Nilsson (2015a) studied the high- and low-Reynolds number models and the DDES and LES models in a flow similar to that in a Francis turbine operating in the part load condition. The hybrid URANS-LES simulations were up to two orders of magnitude more expensive than those with the eddy-viscosity models. They concluded that DDES coupled with the Spalart–Allmaras (DDES-SA) among different hybrid URANS-LES models offers the best results. They also concluded that the DDES-SA model plausibly predicts the highly swirling turbulent flow in hydraulic machinery. The precession happens far from the wall effects, and thus the DDES method is an applicable approach for highly swirling flows (Javadi & Nilsson, 2015a). Javadi and Nilsson (2015b) showed that the DDES method is still sensitive to wall-parallel grid spacing and, in the case of coarse spacing, the method does not switch to the LES mode at all. Wunderer and Schilling (2008) used DES to study active flow control in hydro turbines. They showed that guide vanes, pitching with appropriate frequencies and amplitudes, could reduce the total pressure drop in radial turbines. The linear eddy-viscosity models are not appropriate for such flows because they do not detect the phase lag between the Reynolds stresses tensor and the strain rate. The nonlinear eddy-viscosity and second moment closure models are not robust for such complex flows. Bernardini, Salvadori, Martelli, Paniagua, and Saracoglu (2013) studied the effects of continuous and pulsating coolant blowing from a high pressure turbine vane trailing edge and ended up with a geometrical parameter study of the jets. Liu and Wang (2011) studied the effect of flow separation control using synthetic jets on the performance of a low pressure turbine blade. They showed that the synthetic jet can effectively suppress or even eliminate flow separation on the blade suction surface.

A successful flow control approach should target the momentum deficit near the axis but not close to the wall. In the present study, continuous slot jets with different axial and tangential momentum fluxes ($\rho U_n A \cdot U$) are injected from slots with surface area A at different positions of the runner crown. The purpose is to utilize a small flow rate to manipulate the boundary layer at the crown to prevent the initiation of a vortex rope in the first place. In terms of a massive separation from the crown, a jet located more in the upstream controls the flow more effectively. To achieve this, various continuous slot jets with different angles ($\tan^{-1} U_\theta / U_a$) are injected in different operating conditions. The runner rotational speeds are 400 and 920 rpm, at which the flow field contains a strong vortex rope. The vortex rope counter-rotates with the runner at 400 rpm and co-rotates with the runner at 920 rpm. The jets are injected in a direction opposite to that of the main swirl of the flow. The study is performed with the DDES-SA turbulence model and the results are compared with the results of Javadi and Nilsson (2015a), and Javadi et al. (2016).

2. Flow configuration and computational aspects

The details of the swirl generator and the base cases, without flow control, are given by Bosioc, Muntean, Tanasa, Susan-Resiga, and Vékás (2014). Figure 1(a) shows the studied swirl generator schematically. The swirling flow entering the convergent–divergent section (inlet diameter 100 mm, length 200 mm with the angle of 17°) is very similar to that of a Francis turbine model (Susan-Resiga et al., 2007). This is achieved by using a combination of fixed guide vanes and a runner (hub/shroud diameters 90/150 mm) rotating at a runaway speed of 920 rpm for a discharge of 30 L/s. The guide vanes produce a tangential velocity component, yielding a total pressure decrease from shroud to hub. The axial velocity produced by the

guide vanes is given by

$$U_a(r) = U^G_{a,\text{hub}} \left(\frac{r}{R_{\text{hub}}} \right)^{-\cos^2\alpha}, \quad (1)$$

where r is radial position, and α is the flow angle which is constant after the guide vanes. $U^G_{a,\text{hub}}$ is the axial velocity produced by the guide vanes close to the hub and given by

$$U^G_{a,\text{hub}} = \bar{U}_a \frac{\left(\frac{R_{\text{tip}}}{R_{\text{hub}}}\right)^2 - 1}{\left(\frac{R_{\text{tip}}}{R_{\text{hub}}}\right)^{1+\sin^2\alpha} - 1} \frac{1+\sin^2\alpha}{2}, \quad (2)$$

where $\bar{U}_a$ is bulk velocity in the guide vanes.

The runner blades are designed to distribute the total pressure by increasing the axial velocity near the shroud, with a corresponding deficit near the hub, to mimic the swirl in a Francis turbine operating at partial discharge. The runner acts as a turbine near the hub and as a pump near the shroud, thus providing a corresponding total pressure increase from hub to shroud. The axial velocity exiting the runner is given by

$$U_a(r) = U^R_{a,\text{hub}} \left(\frac{r}{R_{\text{hub}}} \right)^{-\cos^2\beta} + \omega r \frac{\left(\sin 2\beta - (1/2)\sin 2\alpha \sin^2\beta\right)}{1+\cos^2\beta} \times \left[1 - \left(\frac{R_{\text{hub}}}{r} \right)^{1+\cos^2\beta} \right], \quad (3)$$

where ω is the angular velocity of the runner and β is the angle of the flow after the runner. For the details of the derivations see Susan-Resiga, Muntean, Tănasă, and Bosioc (2008).

Since the runner is not shrouded, there is a tip clearance of about 0.008% of the runner radius. A special acquisition and a magneto-rheological brake system were designed and implemented to measure the runner speed and to generate different flow regimes (Bosioc et al., 2014). If the runner rotational speed decreases from 920 via 700 down to 600 rpm, the swirl vanishes and the vortex rope disappears. If the rotational speed further decreases to 400 rpm, the swirl changes direction and the vortex breaks down (Javadi, Bosioc, Nilsson, Muntean, & Susan-Resiga, 2014; Javadi et al., 2016). At these two regimes, 920 and 400 rpm, the vortex rope is well developed and generates large pressure pulsations. The Reynolds number based on the throat bulk velocity and diameter is $\text{Re} = 3.81 \times 10^5$. The experimental survey axes for LDA measurements W0, W1 and W2 (see

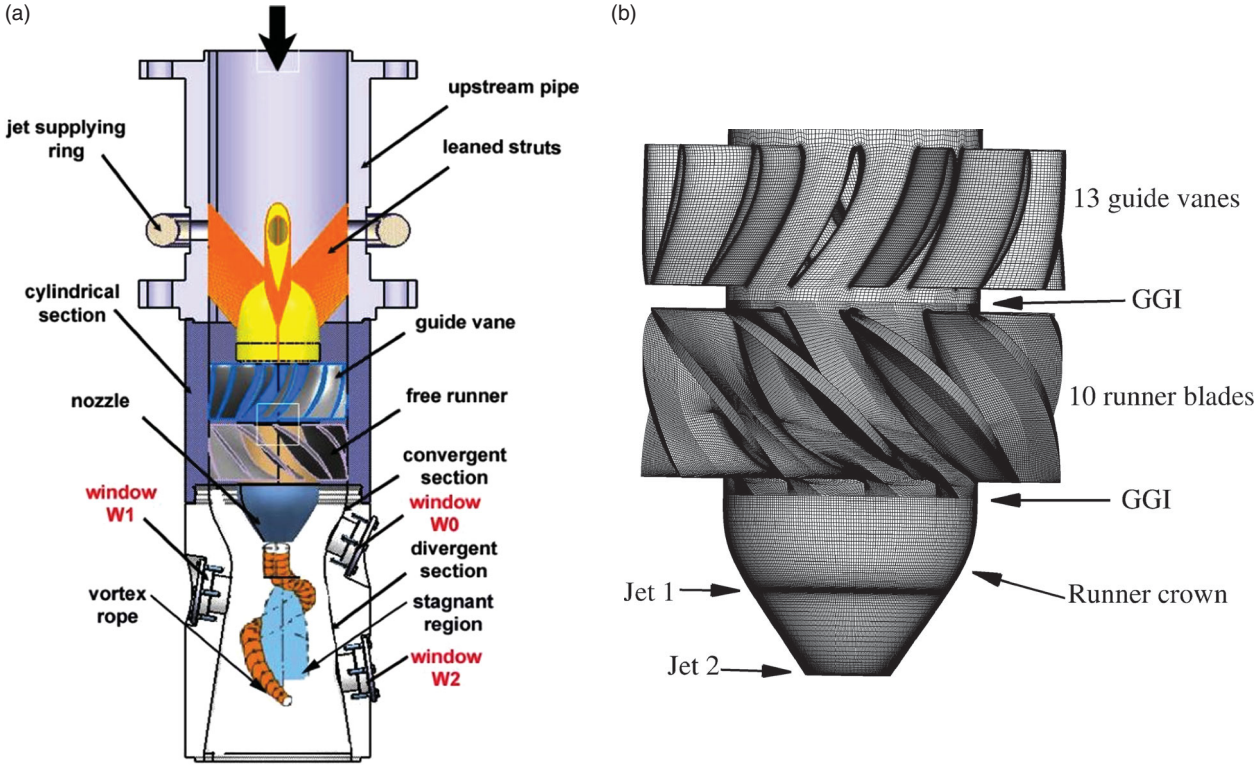

Schematic view of swirl generator. Guide vane, runner blades and the runner crown.

Figure 1. (a) Schematic view of the swirl generator. The results are compared at cross sections W1–W2. (b) Mesh used in the simulations. The positions of Jet 1 and Jet 2 are depicted. Jet 1 is located at the crown tip and Jet 2 is located 20 mm upstream the tip.

Figure 1(a)) are perpendicular to the wall, and start at the wall. The validated numerical results in the two regimes are presented by Javadi et al. (2016) and referred as 'base flow' in the current study. The experimental data are gathered in single-phase (non-cavitating) conditions by keeping the test rig pressurized at a large enough pressure level.

The flow is manipulated using a continuous slot jet at the runner crown, at the two operating conditions 400 and 920 rpm. The effects of the momentum flux, the angle of injection and the location of the slot jet are investigated using seven cases. The two locations of the circumferential slot jet are shown in Figure 1(b). Jet 1 is at the crown tip and Jet 2 is located 20 mm upstream of the tip. The jet emanating components, (radial, tangential, axial) = $(U_r^+, U_\theta^+, U_a^+)$, are normalized by the throat bulk velocity, $U_b = 3.81\ m/s$, and are given in Table 1 together with the jet-to-total flow rate ratio.

The investigation presented herein is performed using the finite-volume method in the FOAM$^{\text{ő}}$-extend-3.0 CFD code. A blended numerical scheme is used for the convective terms. The blended scheme is a combination of linear-upwind differencing in the URANS region and a limited linear Total Variation Diminishing (TVD) scheme with a conformance coefficient in the LES region. The convection term in the LES region is interpolated by 10% linear-upwind differencing and 90% central differencing. The mesh configuration is the same as the base case (Javadi et al., 2016) except for the jet slot as an extra patch and a finer resolution in its vicinity. Figure 1(b) shows the mesh resolution used in the present study, with a total of 16×10^6 cells.

Javadi and Nilsson (2014b) studied a mesh refinement in a flow similar to the current ones and reported that this resolution is fine enough to capture the vortical structures in the field. Furthermore, they showed that the DDES method switches to the LES mode at a reasonable distance from the wall. The wall-normal mesh resolution unit y^+ is defined as

$$y^+ = u^* y/\nu, \quad u^* = \sqrt{\tau_w/\rho}, \quad \tau_w = \mu\left(\frac{\partial u}{\partial y}\right), \quad (4)$$

where u^* is the friction velocity and τ_w is the wall shear stress. The maximum dimensionless wall unit, $y^+_{\max} = 7.2$, in the domain occurs in a small region close to the runner leading edge due to the impingement of the flow, while the mean value is $y^+_{\text{mean}} \sim 1$.

The swirl generator shown in Figure 1(a) including the upstream pipe, guide vanes, runner and conical diffuser was studied using the URANS method (Javadi et al., 2016). The bulk velocity corresponding with the constant discharge was used for inlet in the URANS simulations. The computational domain in this study includes the guide vanes, runner and conical diffuser. The inlet data for velocity and turbulence quantities is extracted from the previously published URANS results (Javadi et al., 2016) upstream of the guide vanes (see Figure 1), and reconstructed by spline curves. For the velocity at the walls, the no-slip condition is applied. The homogeneous Neumann condition is applied for the pressure. The pressure is fixed in a large cell close to the outlet of the draft tube where the pressure fluctuations are expected to be negligible. The turbulence quantities are treated with the homogeneous Neumann condition at the outlet boundary. The *inletOutlet* condition, which is a homogeneous Neumann condition for outgoing flow while blocking the incoming flow, is applied at the outlet boundary for the velocity.

3. Results and discussion

There are two properties that should be addressed to decrease the pressure pulsation and the size of the on-axis recirculation region. First and foremost, the swirl should decrease, i.e. the tangential velocity close to the runner crown should be controlled. Javadi et al. (2016) studied the swirl generator at various flow regimes and demonstrated that the size of the vortex rope, size of the on-axis stagnant region and the pressure pulsation are directly related to the tangential velocity close to the runner crown. Secondly, the wake of the runner crown inevitably forms an on-axis recirculation region, which should be minimized. An applicable control technique

Table 1. Details of slot continuous jets components given by $(U_r^+, U_\theta^+, U_a^+)$.

Operating condition	Jet	Position	Runner rotational speed (rpm)	Q_{jet}/Q	Angle of injection, $\tan^{-1} U_\theta/U_a$ (°)	Momentum flux, $\rho U_n A{\cdot}U$
C1	(0, −2.62, 1.31)	Jet 1	920	0.027	−63	4.0
C2	(0, −2.62, 2.62)	Jet 1	920	0.037	−45	5.5
C3	(0, 2.62, 1.31)	Jet 1	400	0.027	45	4.0
C4	(0, −2.62, 1.31)	Jet 2	920	0.018	−45	2.7
C5	(0, −2.62, 3.93)	Jet 2	920	0.056	−34	25.2
C6	(0, 2.62, 1.31)	Jet 2	400	0.018	63	2.7
C7	(0, 2.62, 3.93)	Jet 2	400	0.056	34	25.2

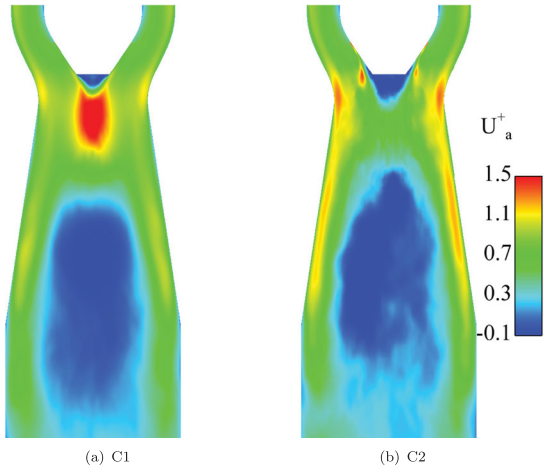

Figure 2. Contour of axial mean velocity, U_a^+, for 920 rpm.

should target both issues and be reasonably practical. Figure 2 shows the axial mean velocity contour in the draft tube. Figure 2(a) shows that the jet in C1 stays attached to the runner crown. If the jet is strong enough to proceed out of the boundary layer, it acts in a manner similar to that of a wall-mounted bluff body and creates its own wake, see Figure 2(b). This feature is undesirable from the point of view of flow control, because it intensifies the wake of the crown.

The survey axes, S^+ at cross sections W0–W2 (see Figure 1), are normalized by the throat radius, $R_{throat} = 0.05$ m, and the velocity is non-dimensionalized by the throat bulk velocity, $U_b = 3.81$ m/s. The survey axes are zero at the wall and perpendicular to the wall. The survey axes extend all the way to the other side of the draft tube at cross sections W1 and W2, where they approach the wall at an angle. The averaging is determined over 15 complete runner revolutions.

Figure 3 shows the axial, U_a^+, and tangential, U_θ^+, mean velocity distributions for 400 rpm and different flow configurations with and without flow control at cross sections W0–W2. The positive axial direction is downward and the runner rotates in the positive direction based on the rule of thumb. The base flow contains a strong vortex, which counter-rotates the runner. To control the vortex rope, the tangential components of the jets are positive. Figure 3 shows that C3 significantly decreases the tangential velocity at cross sections W1 and W2 . The swirl decreases more effectively by a jet at position 1, hereafter Jet 1, than at position 2 (hereafter Jet 2, see positions in Figure 1(b)). It can be seen that the increased axial component of C7 compared to C6 has no significant impact, suggesting that the tangential jet component plays more important role than the axial one. The

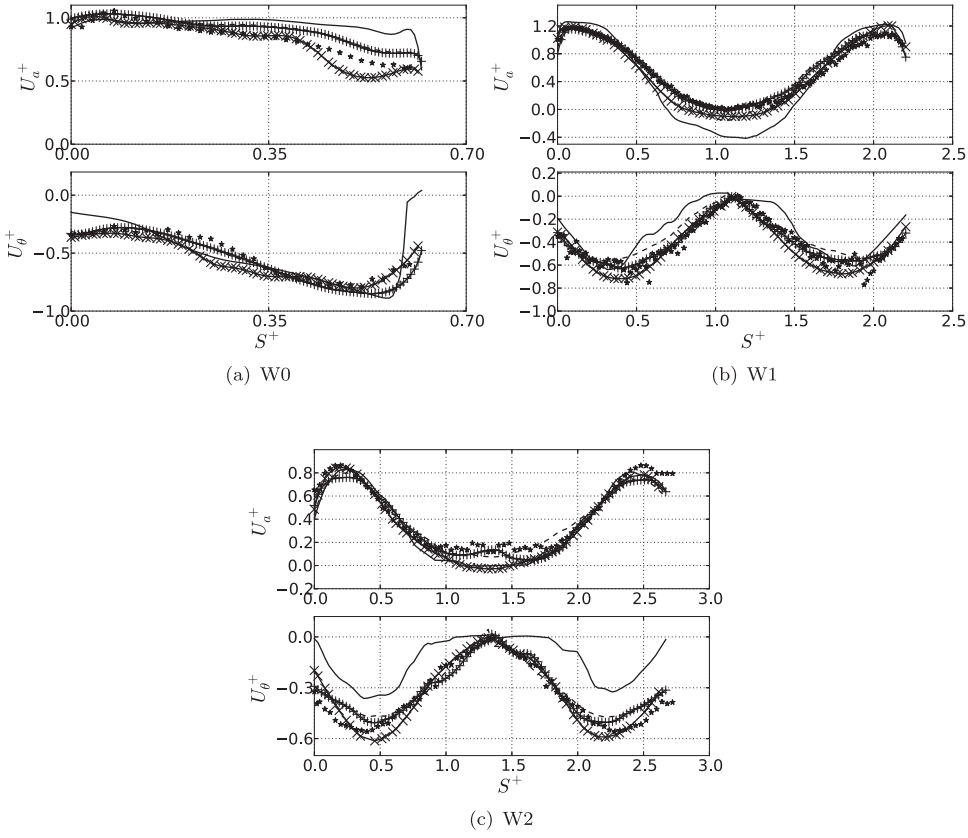

Figure 3. Axial, U_a^+, and tangential, U_θ^+, mean velocity for 400 rpm and different cases: solid line, C3; $+++$, C6; dashed line, C7; $\times\times\times$, no jet; $\star\star\star$, base flow experiment.

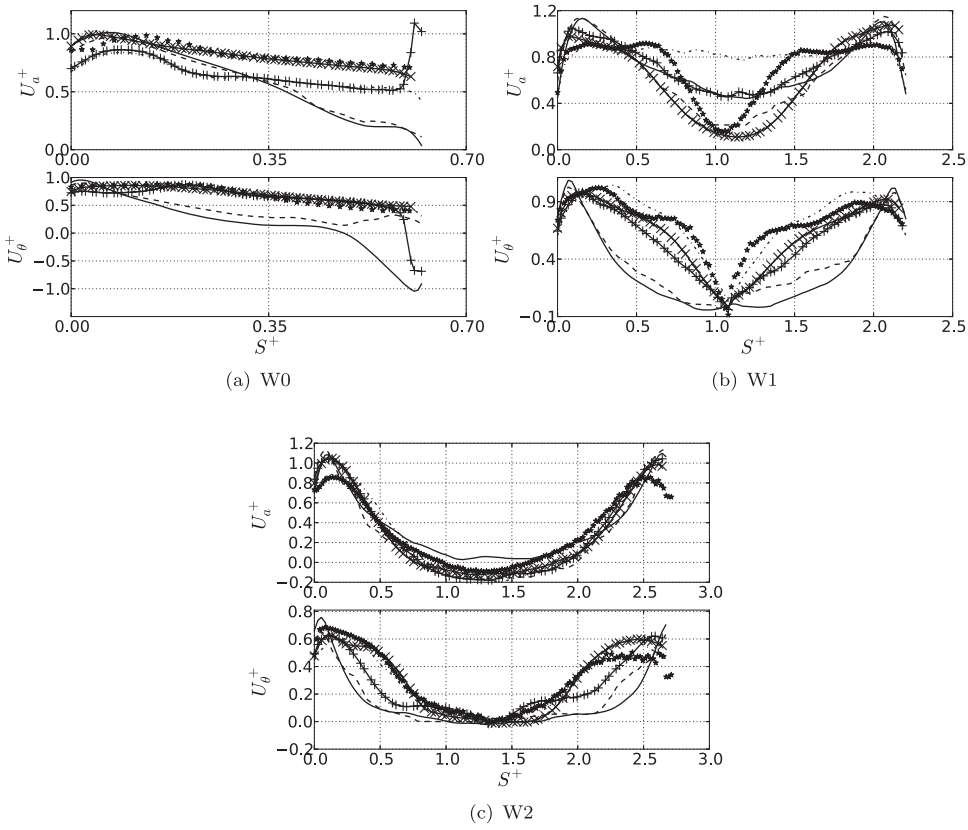

Figure 4. Axial, U_a^+, and tangential, U_θ^+, mean velocity for 920 rpm and different cases: solid line, C1; $+++$, C2; dashed line, C4; dash–dotted line, C5; $\times\times\times$, no jet; $\star\star\star$, base flow experiment.

jets do not control the recirculation region remarkably because the swirl is very strong at this rotational speed.

Figure 4 shows the axial, U_a^+, and tangential, U_θ^+, mean velocity distributions for 920 rpm and different flow configurations with and without flow control at cross sections W0–W2 . The base flow contains a strong vortex, which co-rotates with the runner. To control the vortex, the tangential components of the jets are set negative. Figure 4(a) shows that all jets significantly affect the axial velocity at W1, while C1 and C4 decrease the tangential velocity more remarkably than the other cases. Interestingly, C1 affects the axial velocity more than C4 at W1. Thus, the swirl is decreased by the jets at both positions for 920 rpm. The jets in C2 and C5 do not decrease the tangential velocity at W1. At W2, the jets in C1 and C4 decrease the size of the recirculation remarkably, see Figure 4(b). The jet in C1 stays attached to the hub and increases the momentum in the boundary layer (see Figure 2) and decreases the size of recirculation, while the jet in C2 separates from the runner crown. Jets at position 2 affect the recirculation region less than those at position 1 because the swirl significantly increases in the flow around the crown tip. Thus, the jets at position 2 modify the axial component very much at W1, while there is still a large recirculation region at W2.

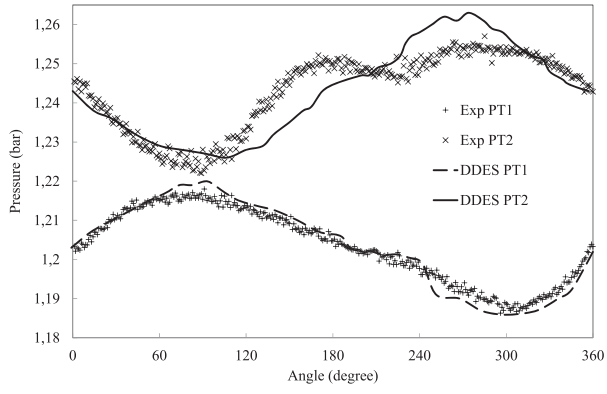

Figure 5. Phase-averaged pressure for 920 rpm of base flow measured at PT1 and PT2 in the draft tube. The profiles of PT1 are moved 0.01 vertical units downwards.

Figure 5 presents the phase-averaged pressure at two pressure taps in the draft tube. The instantaneous dynamic pressure is probed and averaged at 920 rpm for base flow. PT1 is located on the wall at the throat and PT2 is 100 mm axially downstream of the first tap. The profiles show the unsteady periodic behaviour of the flow which is influenced mainly by the vortex rope. The pressure at the two taps are in 180° phase lag. The pressure loss is

0.5 kPa between the two taps, which is reasonably well predicted by DDES-SA.

Figure 6 shows the root mean square of axial, $u'^{+}_{a,\mathrm{rms}}$, and tangential, $u'^{+}_{\theta,\mathrm{rms}}$, velocity fluctuation for 400 rpm and different flow configurations with and without flow control at cross sections W1–W2. It can be seen that the velocity fluctuations are decreased by the jets. The jet in C3 decreases the velocity fluctuations more than the other cases, and the jet in C6 has the lowest effects on the velocity fluctuations, see Figure 6(a). It is worth mentioning that the jets decrease the level of shear between the on-axis recirculation region and the outer part of the flow. The turbulence decay is decreased by the effectiveness of the jets. This means that the decay of the velocity fluctuations in C3 between cross sections W1 and W2 is lower than those of the other cases. The tangential velocity fluctuation in C6 and C7 presents an on-axis peak. The controlled vortex by jets at position 2 is more on-axis than that of jets at position 1 because the issuing jet from the crown tip limits the spatial oscillation of the vortex rope. Thus, it gives an on-axis peak of tangential velocity fluctuation at cross section W2, see Figure 6(b).

Figure 7 shows the root mean square of axial, $u'^{+}_{a,\mathrm{rms}}$, and tangential, $u'^{+}_{\theta,\mathrm{rms}}$, velocity fluctuations for 920 rpm and different flow configurations with and without flow control at cross sections W1-W2. It can be seen that the jets decrease the velocity fluctuations at W1, see Figure 7(a), in the same trend as discussed for the mean velocity distribution. At W1, the axial velocity fluctuation highly is decreased by jets in C1 and C4 and the tangential velocity fluctuation decreases by jets in C1, C2 and C4, see Figure 7(a). The jet in C5 has the least effects on the velocity fluctuations among the cases. Jets at position 1 affect the size of the recirculation region and the velocity fluctuations more than those of jets at position 2. The more effective jet presents a lower level of decay of velocity fluctuations in the draft tube.

Figures 8 and 9 show the q-criterion for different jets for 400 and 920 rpm, respectively. In the case of 'No jet' there is a strong vortex rope, see Figures 8(a) and 9(a).

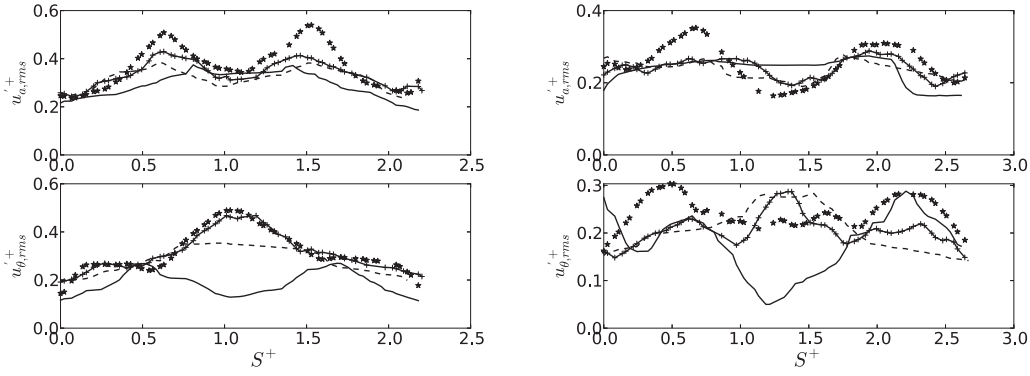

(a) W1 (b) W2

Figure 6. Root mean square of axial, $u'^{+}_{a,\mathrm{rms}}$, and tangential, $u'^{+}_{\theta,\mathrm{rms}}$, velocity fluctuation for 400 rpm and different cases: solid line, C3; + + +, C6; dashed line C7; ⋆ ⋆ ⋆, jet.

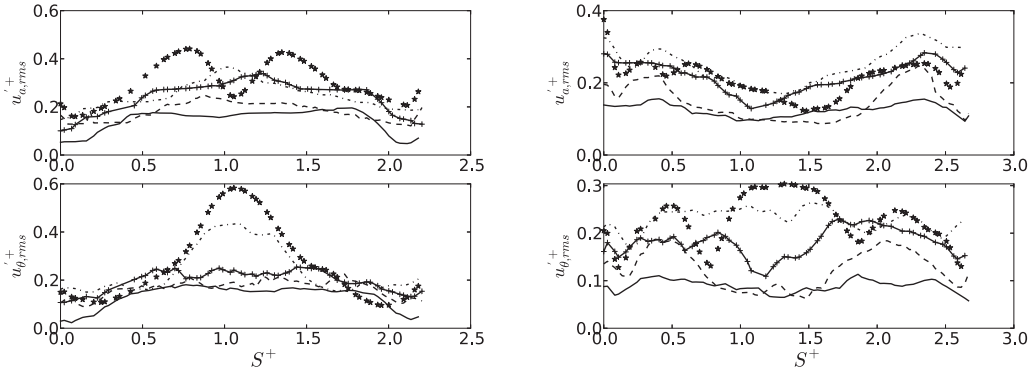

(a) W1 (b) W2

Figure 7. Root mean square of axial, $u'^{+}_{a,\mathrm{rms}}$, and tangential, $u'^{+}_{\theta,\mathrm{rms}}$, velocity fluctuation for 920 rpm and different cases: solid line, C1; + + +, C2; dashed line, C4; dash–dotted line, C5; ⋆ ⋆ ⋆, jet.

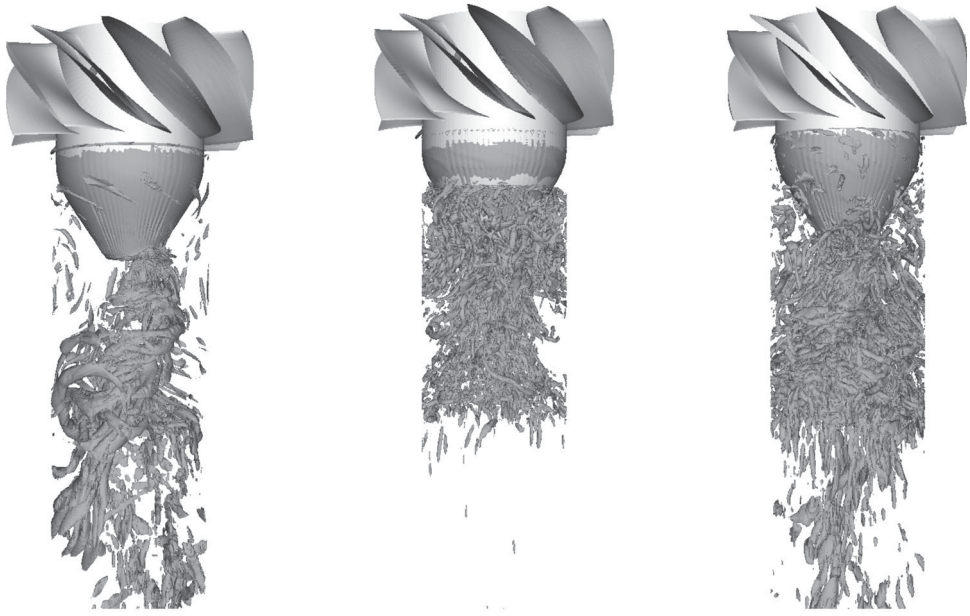

(a) No jet (b) C3 (c) C7

Figure 8. Iso-surface of q-criterion, $q = 50{,}000$, for different jets, 400 rpm.

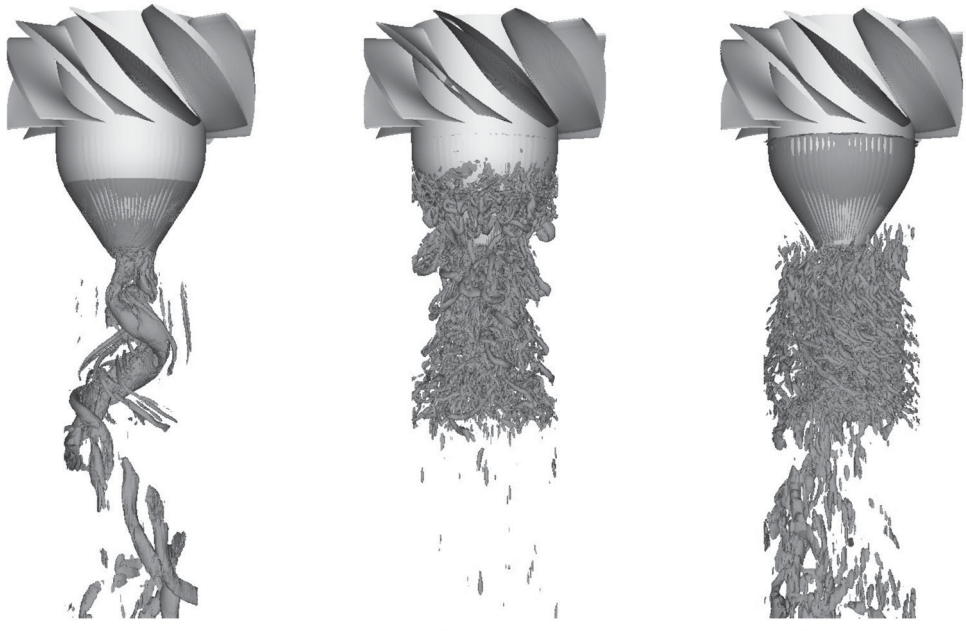

(a) No jet (b) C1 (c) C5

Figure 9. Iso-surface of q-criterion, $q = 50{,}000$, for different jets and 920 rpm.

The flow control technique affects the size of the vortex rope remarkably. Jets at position 1 reduce the size of the vortex rope significantly, see Figures 8(b) and 9(b). Jets at position 2 reduce the size of the vortex rope while still keeping its plunging motion, see the lower parts of Figures 8(c) and 9(c).

Figure 10 shows the fast Fourier transform of the dynamic pressure probed at the on-axis point of W2 for 400 and 920 rpm. The frequency of the vortex rope in 'No jet' and 400 rpm is $f/f_{\text{runner}} \sim 1.5$, see Figure 10(a). At this operating condition, the plunging motions and disintegration of the vortex rope have low pressure amplitudes

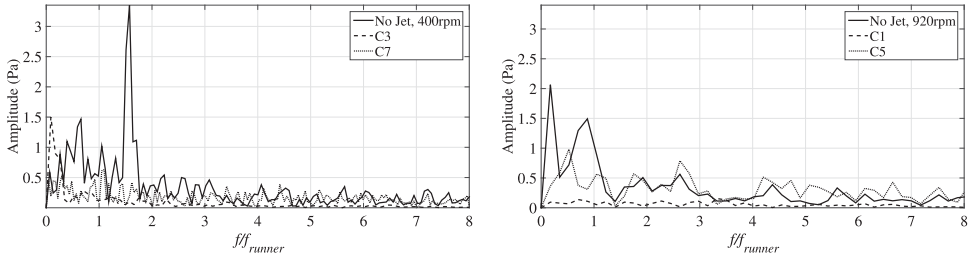

(a) 400rpm (b) 920rpm

Figure 10. FFT of dynamic pressure probed at the on-axis point of W2 for 400 and 920 rpm.

and frequencies, see Figure 10(a), in the range $f/f_{\text{runner}} = [0-1]$. The flow control considerably decreases the amplitude of the pulsations. There is no dominant frequency in C7, while C3 still shows a peak at a very low frequency, see Figure 10(a). The frequency of the vortex rope in 'No jet' and 920 rpm is $f/f_{\text{runner}} \sim 1$. At this operating condition, the plunging motion has a strong pressure pulsation at a low frequency, see Figure 10(b). The flow control considerably decreases the pressure amplitude of the structures. The flow in C1 shows very small pressure pulsations. The vortex rope for 400 rpm is stronger than that for 920 rpm. The jets with stronger components would affect the recirculation region more remarkably at 400 rpm.

Figures 11 and 12 show the temporal power spectral density at the on-axis point of W2 for 400 and 920 rpm, respectively. Figure 11(a) shows that there is a peak at $f/f_{\text{runner}} \sim 1.5$ due to the strong vortex rope. There are other periodicities related to the wakes of the blades at $f/f_{\text{runner}} \sim 10$. Figure 11(b) confirms that there is no vortex rope in C3. Figures 11(c) and 11(d) show a peak in the vortex rope region which is less strong than that for the 'No jet' condition. It is noteworthy that the jets at position 2 decrease the size of the vortex rope but do not remove it. Instead, C6 and C7 create lots of small-scale structures with high frequencies in the dissipation regions. Figure 12 shows that the jets decrease the energy of the vortex rope significantly. Since the level of swirl for 920 rpm is lower than that for 400 rpm, the jets are capable of remarkably decreasing the tangential velocity. Table 2 shows the integral length scale in both operating conditions and for all the cases, based on an integration of the auto-correlation over the entire temporal domain. The auto-correlation is defined

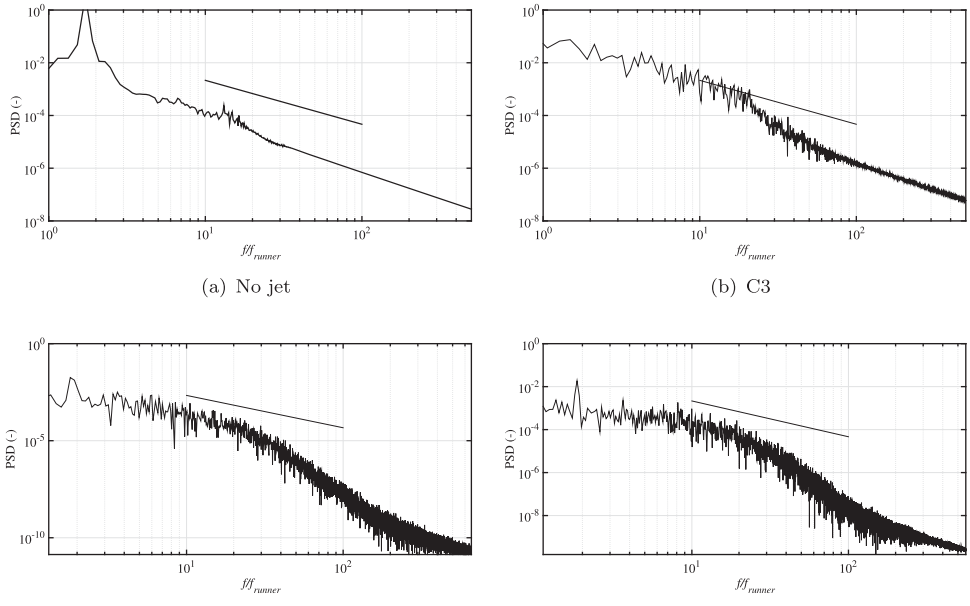

(a) No jet (b) C3

(c) C6 (d) C7

Figure 11. Temporal power spectral density probed at the on-axis point of W2, 400 rpm.

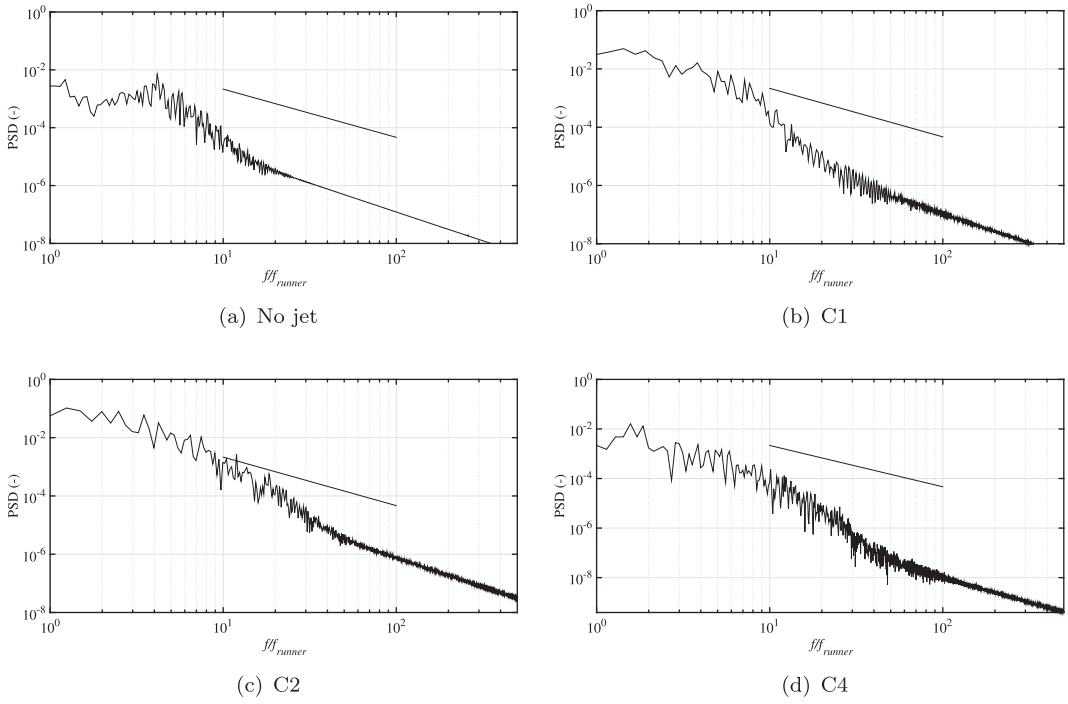

Figure 12. Temporal power spectral density probed at the on-axis point of W2, 920 rpm.

Table 2. Integral length scale for different operating conditions.

Operating condition	No jet, 400 rpm	No jet, 920 rpm	C1	C2	C3	C4	C5	C6	C7
L_{int}(cm)	12	9.5	1.5	3.3	7.8	8.4	7.8	7.2	9.8

by

$$\text{ACF}(\hat{t}) = \overline{u'(t)u'(t+\hat{t}\,)}, \tag{5}$$

where u' is velocity fluctuation and $\hat{t}$ is the time separation. If the mean flow is steady, the 'time direction' is homogeneous and ACF is independent of time. The normalized ACF reads

$$\text{ACF}^{\text{norm}}(\hat{t}) = \frac{1}{\overline{u'^2}}\overline{u'(t)u'(t+\hat{t}\,)}. \tag{6}$$

In this analogy to the integral length scale, L_{int}, the *integral timescale* is defined as

$$T_{\text{int}} = \int_0^\infty \text{ACF}^{\text{norm}}(\hat{t}\,)\,\mathrm{d}\hat{t}. \tag{7}$$

The time length scale represents the timescale of large energy-containing eddies. The vortex rope for 400 rpm has an integral length scale of $L_{\text{int}} = 12\,cm$, which is larger than $L_{\text{int}} = 9.5$ cm for 920 rpm. Thus, the 400 rpm condition needs stronger jets to control the vortex rope and the recirculation region. It can be seen that the integral length scales are reduced. The smallest scale is in C1 with $L_{\text{int}} = 1.5\,cm$.

4. Conclusions

The vortex rope in flows very similar to those of a Fracis turbine is controlled by continuous circumferential slot jets at the runner crown. The numerical results of flow fields with active flow control using DDES-SA are compared with validated numerical results without active flow control. Seven jets are studied, with different momentum fluxes, angle of injection and positions. It is shown that

- for 400 rpm, C3, the jet with $(U_r^+, U_\theta^+, U_a^+) = (0, 2.62, 1.31)$ at position 1, shrinks the vortex rope more than do C6 with (0, 2.62, 1.31) and C7 with (0, 2.62, 3.93) at position 2;
- for 920 rpm, C1 is the jet with (0, −2.62, 1.31) and C2 is the jet with (0, −2.62, 2.62) at position 1. They shrink the vortex rope more effectively than do C4 with (0, −2.62, 1.31) and C5 with (0, −2.62, 3.93) at

position 2, because the swirl at position 2 is stronger than that at position 1;
- the jet at position 1 decreases the pulsations and possibly prevents vortex breakdown, while the jet at position 2 is less effective;
- the tangential component of the jet is more important than the axial component of the jet in making the jet more effective at flow control.

The jet in C1 is the most effective case in preventing vortex breakdown and mitigating the pulsations, and thus decreasing the velocity fluctuations. Hence, injecting a continuous circumferential slot jet in a direction opposite to that of the main swirl of the flow is remarkably effective in both preventing vortex breakdown and shrinking the vortex rope. Momentum flux, jet angle and jet position are decisive factors in the effectiveness of the technique. These factors depend on the operating condition and should be optimized by a feedback-control system, which is for future work.

Disclosure statement

No potential conflict of interest was reported by the authors.

Funding

The research presented was carried out as a part of the Swedish Hydropower Centre (SVC). SVC was established by the Swedish Energy Agency, EnergiForsk and Svenska Kraftnät, together with Luleå University of Technology, The Royal Institute of Technology, Chalmers University of Technology and Uppsala University (http://www.svc.nu). The computational facilities are provided by C^{3}SE, the centre for scientific and technical computing at Chalmers University of Technology, and the Swedish National Infrastructure for Computing (SNIC).

References

Bernardini C., Salvadori S., Martelli F., Paniagua G., & Saracoglu B. H. (2013). Pulsating coolant ejection effects downstream of supersonic trailing edge. *Engineering Applications of Computational Fluid Mechanics*, *7*(2), 250–260. doi:10.1080/19942060.2013.11015468

Bosioc A. I., Muntean S., Tanasa C., Susan-Resiga R., & Vékás L. (2014). Unsteady pressure measurements of decelerated swirling flow in a discharge cone at lower runner speeds. *IOP Conference Series: Earth and Environmental Science*, *22*(3), Unsteady and Transient Phenomena. Retrieved from http://stacks.iop.org/1755-1315/22/i=3/a=032008

Javadi A., Bosioc A., Nilsson H., Muntean S., & Susan-Resiga R. (2014). Velocity and pressure fluctuations induced by the precessing helical vortex in a conical diffuser. *IOP Conference Series: Earth and Environmental Science*, *22*(3), Unsteady and Transient Phenomena. Retrieved from http://stacks.iop.org/1755-1315/22/i=3/a=032009

Javadi A., Bosioc A., Nilsson H., Muntean S., & Susan-Resiga R. (2016). Experimental and numerical investigation of the precessing helical vortex in a conical diffuser, with rotor–stator interaction. *ASME Journal of Fluids Engineering*. doi:10.1115/1.4033416

Javadi A., & Nilsson H. (2014a). A comparative study of scale-adaptive and large-eddy simulations of highly swirling turbulent flow through an abrupt expansion. *IOP Conference Series: Earth and Environmental Science*, *22*(2), Unsteady and Transient Phenomena. Retrieved from http://stacks.iop.org/1755-1315/22/i=2/a=022017

Javadi A., & Nilsson H. (2014b). LES and DES of swirling flow with rotor–stator interaction. *Progress in Hybrid RANS-LES Modelling*, *130*, 457–468.

Javadi A., & Nilsson H. (2015a). Time-accurate numerical simulations of swirling flow with rotor–stator interaction. *Flow, Turbulence and Combustion*, *95*, 755–774.

Javadi A., & Nilsson H. (2015b). LES and DES of strongly swirling turbulent flow through a suddenly expanding circular pipe. *Computers and Fluids*, *107*, 301–313. doi:10.1016/j.compfluid.2014.11.014

Kjeldsen M., Olsen K. M., Nielsen T., & Dahlhaug O. G. (2006). *Water injection for the mitigation of draft-tube pressure pulsations*. Presented at the IAHR international meeting of WG on cavitation and dynamic problems in hydraulic machinery and systems, Barcelona, Spain.

Liu X., & Wang X. (2011). Performance improvement of low pressure turbine blade by using synthetic jets. *Engineering Applications of Computational Fluid Dynamics*, *5*(4), 445–458. doi:10.1080/19942060.2011.11015385

Menter F. R., & Egorov Y. (2010). The scale-adaptive simulation method for unsteady turbulent flow predictions. Part 1: Theory and model description. *Flow, Turbulence and Combustion*, *85*, 113–138.

Nishi M., Wang X. M., Yoshida K., Takahashi T., & Tsukamoto T. (1996). *An experimental study on fins, their role in control of the draft tube surging*. In *Hydraulic Machinery and Cavitation* (pp. 905–914). Dordrecht, The Netherlands: Hydraulic Machinery and Cavitation.

Rusak Z., Granata J., & Wang S. (2015). An active feedback flow control theory of the axisymmetric vortex breakdown process. *Journal of Fluid Mechanics*, *774*, 488–528.

Spalart P. R. (2009). Detached-eddy simulation. *Annual Review of Fluid Mechanics*, *41*(3), 181–202.

Spalart P. R., Deck S., Shur M. L., Squires K. D., Strelets M. Kh., & Travin A. (2006). A new version of detached-eddy simulation, resistant to ambiguous grid densities. *Theoretical and Computational Fluid Dynamics*, *20*(3), 181–195.

Spalart P., Jou W., Strelets M., & Allmaras S. (1997). *Comments on the feasibility of LES for wings and on a hybrid RANS-LES approach*. In *Advances in DNS-LES, Proceedings of the1st AFOSR international conference on DNS-LES*, 4–8 August 1997, Ruston, LA. Columbus, OH: Greyden Press. Retrieved from http://www.cobaltcfd.com/pdfs/DES97.pdf

Susan-Resiga R., Muntean S., Bosioc A. I., Stuparu A., Milos T., & Baya T. (2007). *Swirling flow apparatus and test rig flow control in hydraulic turbines discharge cone*. Presented at the 2nd IAHR international meeting of the workgroup on cavitation and dynamic problems in hydraulic machinery and systems, Timisoara, Romania.

Susan-Resiga R., Muntean S., Hasmatuchi V., Anton I., & Avellan F. (2010). Analysis and prevention of vortex breakdown

in the simplified discharge cone of a Francis turbine. *ASME Journal of Fluids Engineering*, *132* (5), 051102-1–051102-15. Retrieved from http://dx.doi.org/10.1115/1.4001486

Susan-Resiga R., Muntean S., Tănasă C., & Bosioc A. (2008). *Hydrodynamic design and analysis of a swirling flow generator*. In *Proceedings of the 4th German–Romanian workshop on turbomachinery hydrodynamics (GROWTH-4)*, Stuttgart, Germany.

Susan-Resiga R., Vu T. C., Muntean S., Ciocan G. D., & Nennemann B. (2006). *Jet control of the draft tube vortex rope in Francis turbines at partial discharge*. In *Proceedings of the 23rd IAHR symposium on hydraulic machinery and systems*, Yokohama, Japan.

Tănasă C., Bosioc A., Muntean S., & Susan-Resiga R. (2013). Flow-feedback method for mitigating the vortex rope in decelerated swirling flows. *ASME Journal of Fluids Engineering*, *135*(6), 1–11.

Wunderer R., & Schilling R. (2008). *Numerical simulation of active flow control in hydro turbines*. Presented at the 12th international symposium on transport phenomena and dynamics of rotating machinery (ISROMAC-12).